

# Statistics of geometrical invariants of magnetic field gradient tensors in the turbulent magnetosheath based on magnetospheric multiscale mission

Cite as: Phys. Fluids **35**, 025107 (2023); <https://doi.org/10.1063/5.0134514>

Submitted: 11 November 2022 • Accepted: 12 January 2023 • Accepted Manuscript Online: 12 January 2023 • Published Online: 02 February 2023

 Yong Ji (纪勇),  Chao Shen (沈超), Lan Ma (马兰), et al.



View Online



Export Citation



CrossMark

## ARTICLES YOU MAY BE INTERESTED IN

[Tripolar guide magnetic fields due to island coalescence in solar wind current sheets: Simulation and theory](#)

Physics of Plasmas **29**, 112905 (2022); <https://doi.org/10.1063/5.0102906>

[Hybrid simulations of the decay of reconnected structures downstream of the bow shock](#)

Physics of Plasmas **30**, 012902 (2023); <https://doi.org/10.1063/5.0129084>

[Numerical study of Richtmyer-Meshkov Instability of a flat interface driven by perturbed and reflected shock waves](#)

Physics of Fluids (2023); <https://doi.org/10.1063/5.0137389>



## Physics of Fluids

Special Topic: Paint and Coating Physics

Submit Today!

# Statistics of geometrical invariants of magnetic field gradient tensors in the turbulent magnetosheath based on magnetospheric multiscale mission

Cite as: Phys. Fluids **35**, 025107 (2023); doi: 10.1063/5.0134514

Submitted: 11 November 2022 · Accepted: 12 January 2023 ·

Published Online: 2 February 2023



View Online



Export Citation



CrossMark

Yong Ji (纪勇), Chao Shen (沈超),<sup>a)</sup> Lan Ma (马兰), Nian Ren (任年), and Nisar Ahmad

## AFFILIATIONS

School of Science, Harbin Institute of Technology (Shenzhen), Shenzhen 518055, People's Republic of China

<sup>a)</sup> Author to whom correspondence should be addressed: [shenchao@hit.edu.cn](mailto:shenchao@hit.edu.cn)

## ABSTRACT

Geometrical invariants of magnetic field gradient tensors are used to classify the topological structures of a magnetic field. This study presents a statistical analysis on the geometrical invariants of magnetic field gradient based on high-quality data measured by magnetospheric multiscale mission in turbulent magnetosheath. The method for the classification of velocity field topologies cannot be applied to magnetic field with strong intensity directly because the magnetic field cannot be transformed to zero by selecting a co-moving reference frame in which the velocity is zero. During a strong magnetic field, flux ropes and tubes are the most possible magnetic structures. Statistics in the plane formed by geometrical invariants show that about 23% are force-free structures comprised of 20.5% flux tubes and 79.5% flux ropes. The remaining actively evolved structures are comprised of 30% flux tubes and 70% flux ropes. Moreover, the conditional average of current density and Lorentz force decomposition in geometrical invariants plane are investigated. The results show that flux ropes carried more current density than flux tubes for the same geometrical invariants, and flux ropes tend to associate with magnetic pressure force and flux tubes tend to associate with magnetic tension.

Published under an exclusive license by AIP Publishing. <https://doi.org/10.1063/5.0134514>

## I. INTRODUCTION

Plasma turbulence is ubiquitous in the interstellar medium, the atmosphere of stars, the Earth's magnetosphere, and nuclear fusion devices.<sup>1</sup> It plays an important role in transferring energy and momentum between flow and magnetic field as well as energy cascades from large toward small spatial scales.<sup>2</sup> Understanding space plasma turbulence is of applicable value, since turbulence is related to solar energetic particles,<sup>3</sup> cosmic rays,<sup>4</sup> geomagnetic storm,<sup>5</sup> and enhancement of MeV electron flux in radiation belt.<sup>6</sup> Highly perturbed magnetosheath formed by the interaction of supersonic solar wind on geomagnetosphere is an ideal natural laboratory to study the mechanism of collisionless plasma turbulence.<sup>7</sup> Based on observations of magnetosheath, researchers have made considerable progress on plasma turbulence, revealing the mechanism of magnetic reconnection in electron scale,<sup>8,9</sup> identifying the structures in terms of the Vlasov equation,<sup>10</sup> and the statistics of kinetic dissipation during turbulence.<sup>11–13</sup>

Coherent structures are universal in both space and laboratory plasma turbulence. Even in homogeneous isotropic hydrodynamic

turbulence, there appears to be intermittent vortex structures.<sup>14</sup> The solar wind is a plasma turbulence system where the magnetic field structures had been well studied, such as neutral X lines,<sup>9</sup> current sheet,<sup>15</sup> and field discontinuities.<sup>16</sup> Usually, magnetic frozen condition breaks at X lines and magnetic field line decouples with fluid motion, associated with the heating of charged particles.<sup>5</sup> Numerical study shows that coherent current sheet structures span a wide range of scales and are responsible for heating and dissipation.<sup>17</sup> Solar wind discontinuities modulate the turbulence state in magnetosheath and the interaction of the solar wind vs the magnetosphere.<sup>16</sup> In addition, not all coherent structures are dynamical and enhance energy transformation or dissipation. Force-free magnetic field configurations, in which magnetic field is parallel to the current density, can be stable and just advected by flow.<sup>18</sup> It is a prerequisite to diagnose these magnetic field structures for understanding the mechanism of plasma turbulence in magnetosheath. The magnetic field gradient tensor is one term in the dynamical equation describing the evolution of the turbulent velocity field that should be paid attention to.

The velocity gradient tensors play an important role in the identification of the vortex structures<sup>19–21</sup> and turbulent energy dissipation.<sup>22</sup> The related methods for velocity gradient tensors can be extended to magnetic gradient tensors of plasma turbulence. Recently, the general classification of three-dimensional velocity fields<sup>23</sup> was applied to analyze multipoint *in situ* observations of the solar wind and magnetosheath.<sup>24–27</sup> The coherent structures in the solar wind were identified based on the analysis of the geometrical invariants of magnetic field gradient tensor.<sup>26</sup> Hnat *et al.*<sup>26</sup> found that the structures are mainly comprised of 3D plasmoids ( $\sim 1/3$ ), flux ropes ( $\sim 3/5$ ), and 3D X-point ( $\sim 1/5$ ), supporting strong turbulence existing in solar wind.<sup>28</sup> The gradient construction method has been performed in the co-ordinates of the volumetric tensor eigenvectors and thus accounts for possible deformations of the irregular multiple point spacecraft tetrahedron.<sup>29</sup> However, it should be noted that, only when the isotropic condition satisfies, the method used to classify the topology of velocity field is suitable for analyzing the magnetic field. Blackburn *et al.*<sup>30</sup> pointed out that the classification method is based on Lagrangian viewpoint. Under a Lagrangian frame, local velocity is zero, and each point can be regarded as a critical point, so that critical point terminology can be used to classify the topology. For magnetic field, the background field cannot be removed by using a Lagrangian frame, which means both magnetic field and its gradient determines topology of field lines. Moreover, Quattrociochi *et al.*<sup>31</sup> derived the evolution equations of the geometrical invariants of magnetic field gradient tensor and show that the term including magnetic field cannot be neglected under non-homogeneous cases. The magnetosheath is a transitional region from the solar wind to the magnetosphere, which is a non-homogeneous case, and it is meaningful to investigate the statistical properties of the geometrical invariants of magnetic field gradient in this region.

Along with the execution of a multipoint exploration program for the geomagnetosphere,<sup>32,33</sup> innovative and systematic algorithms to calculate the first and second order gradient of magnetic field have been put forward and developed.<sup>29,34–38</sup> The algorithm has been successfully applied to analyze the structure of the current sheet, geomagnetic tail,<sup>29,34,35</sup> ring current,<sup>39</sup> and the curvature of turbulent magnetic field in magnetosheath.<sup>40</sup> Combining multiple analysis methods and *in situ* observations of Magnetospheric Multiscale (MMS) mission, we analyze the magnetic structures in magnetosheath based on the classification of magnetic topology.

Magnetospheric Multiscale(MMS) mission conducted by NASA is the latest multipoint detection program for revealing the law of magnetic reconnection.<sup>8</sup> MMS composed of four identical spacecraft with 11 instruments having 25 sensors. Relying on these precise sensors, energetic charged particles, statistical properties of plasma, and electric and magnetic fields can be measured with unprecedentedly high—on the order of milliseconds—time resolution and accuracy.<sup>8,41</sup> To resolve the reconnection mechanism in electron scale, the orbit of four MMS spacecraft in tetrahedra formation with about 10–160 km<sup>8</sup> enables researchers to calculate the precise spatial gradient of physical quantities by means of a multiple point algorithm.<sup>29</sup> After getting the data through MMS, the spatial gradient of velocity and magnetic field can be analyzed. In summary, the data from MMS and the multiple analysis methods enable us to study different structures in magnetosheath turbulence.

In this work, we aim to investigate the geometrical invariants of magnetic field gradient tensor with a set of MMS measurements in magnetosheath. First, the gradient tensor of magnetic field is determined by using the multiple point method;<sup>29</sup> second, the statistical properties of the geometric invariants of the magnetic field gradient tensor with and without Lorentz force are evaluated and compared with the results obtained by Hnat *et al.*<sup>26</sup> in the solar wind. Finally, the conditional mean value of current density and Lorentz force decomposition in geometrical invariants plane are analyzed.

## II. METHOD

### A. Multiple point method

This study calculates the spatial gradient of  $\mathbf{B}$  by using the multiple point method developed by Shen *et al.*<sup>29</sup> The method was designed to determine the spatial gradient at the mesocenter of the multiple point. First, the volume tensor  $R_{nl} \equiv \frac{1}{4} \sum r_{\alpha l} r_{\alpha n}$  is determined, where  $r$  denotes the position co-ordinates with respect to mesocenter,  $\alpha$  denotes the number of crafts ranging from one to four for MMS, subscripts  $l$  and  $n$  denote the components of  $x - y - z$  co-ordinates. Second, the gradient tensor of magnetic field vector  $A_{mn}^0$  is determined from the following equation:

$$A_{mn}^0 = \frac{1}{4} \sum_{\alpha=1}^4 B_{\alpha m} r_{\alpha l} R_{nl}^{-1}, \quad (1)$$

where  $B_{\alpha m}$  denotes the measurement of  $m$ -component of  $\mathbf{B}$  at  $\mathbf{r}_{\alpha}$ . Note that  $R_{nl}$  will become abnormal when the polyhedron of the spacecraft is distorted considerably. For the purpose of avoiding the error caused by abnormal  $R_{nl}$ , Shen *et al.*<sup>29</sup> derived the gradient in the eigenspace of  $R_{nl}$ . More details could be found in Ref. 29. In addition, the residual error of  $A_{ii}^0$  that should be zero according to no divergence of magnetic field was also corrected by Shen *et al.*,<sup>34</sup>

$$A_{mn} = A_{mn}^0 + \lambda R_{mn}^{-1}, \quad (2)$$

where  $\lambda = -A_{ii}^0/R_{ii}^{-1}$  is a Lagrangian multiplier. Equation (2) will be used to determine the gradient of magnetic field in this study.

### B. Geometrical invariants of magnetic field gradient tensor

Gradient fields of magnetic field characterize the local quantitative and qualitative behavior of MHD flows. According to the linear approximation, the magnetic field  $\mathbf{B}(\mathbf{r}, t)$  surrounding an arbitrary point ( $\mathbf{r}_0$ ) in MHD flow can be expressed as

$$B_j(\mathbf{r}, t) = B_j(\mathbf{r}_0, t) + A_{jn}(\mathbf{r}_0, t)(x_n - x_{0n}), \quad (3)$$

where  $A_{jn}$  is the element of gradient tensor ( $\mathbf{A}$ ) of  $\mathbf{B}$  that can be computed based on Eq. (2). The geometrical invariants of  $\mathbf{A}$  are defined as

$$P = -tr(\mathbf{A}) = 0, \quad Q = -\frac{1}{2}tr(\mathbf{A}^2), \quad R = -\frac{1}{3}tr(\mathbf{A}^3), \quad (4)$$

which are unchanged under the rotation operation of the frame. Here,  $P = 0$  is attributed to non-divergence of the magnetic field. Note that the geometrical invariants also determine the eigenvalues  $\lambda_i \in \mathbb{C}$  of  $\mathbf{A}$  in terms of the characteristic equation  $|\mathbf{A} - \lambda_i \mathbf{I}| = \lambda_i^3 + P\lambda_i^2 + Q\lambda_i + R = 0$ . It can be shown that in the  $(R, Q)$  plane, the surface determined by  $D \equiv 27/4R^2 + Q^3 = 0$  divides the eigenvalues into

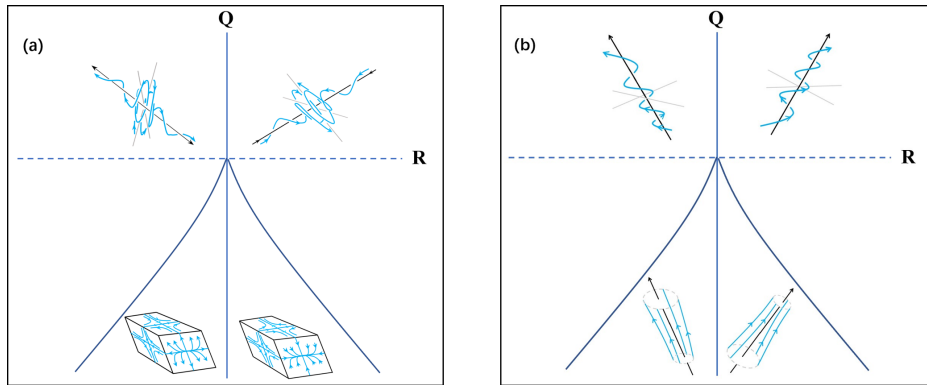


FIG. 1. Expected sketches of the magnetic field line typologies in each quadrant of the invariants' plane with (a) weak magnetic field and (b) strong magnetic field.

two categories.<sup>26</sup> When  $D > 0$ , two eigenvalues of  $A$  are complex and one is real, and when  $D < 0$ , three eigenvalues are real. In addition, the current density flux can also be calculated from the  $A$  via Faraday's law  $\nabla \times \mathbf{B} = \mathbf{j}$ , where the permeability is regarded as a unit here. The mean current density magnitude  $\langle j \rangle$  of all samples is used to make  $R$  and  $Q - nR = R/\langle j^2 \rangle^{3/2}$ ,  $nQ = Q/\langle j^2 \rangle$  non-dimensional.

### C. Typology of magnetic field lines

Figure 1 shows the expected types of magnetic field lines in the plane formed by the invariants  $Q$  and  $R$ . The curve corresponds to  $D = 0$  that is used to classify the eigenvalues of  $A$ . Figure 1(a) shows the typologies for the critical point at which magnetic strength is weak or can be regarded as zero, which are adapted from the classification of velocity field.<sup>42</sup> In the topological study of three-dimensional flow by Chong *et al.*,<sup>23</sup> the typologies in  $D > 0, R < 0$  region (upper left) are called stable focus/stretching, in  $D > 0, R > 0$  region (upper right) unstable focus/compressing, in  $D < 0, R < 0$  region (lower left) stable node/saddle/saddle, and in  $D < 0, R > 0$  region (lower right) unstable node/saddle/saddle. For magnetic field lines, Hnat *et al.* put forward a simpler classification showing invariants with  $D > 0, R \sim 0$  are quasi-2D flux structures,  $D > 0, |R| \gg 0$  corresponding for plasmoids and  $D < 0$  corresponding to 3D reconnection structures. We want to emphasize that Fig. 1(a) can describe all structures of velocity field because each point of flow field can be a critical point if we choose to observe the co-moving frame with flow. However, for magnetic field, the magnetic strength cannot be removed in the co-moving frame and it also plays a role in the dynamical equation of magnetic field gradients.<sup>25,31</sup> Therefore, the situations with non-negligible

magnetic strength should be considered individually. Figure 1(b) shows the typologies of magnetic field lines that cannot be regarded as critical points. Assuming that the guide field is strong and the variation of magnetic strength in the field direction is small within the scale of MMS tetrahedra, there are two kinds of typologies, flux rope for  $D > 0$  and flux tube for  $D < 0$ . The value of  $R$  determines the left-handed or right-handed for flux rope, narrowing or expanding for flux tube, which also depends on the direction of the magnetic field. This study mainly focuses on data with a strong guide field, which corresponds to the typologies shown in Fig. 1(b).

### III. DATA

Five datasets are selected from measurements during this study. Time intervals and the spacecraft positions of selected data are shown in Table I. Since this study intends to investigate geometrical invariants of magnetic field gradient and associated work done by the Lorentz force, magnetic field data measured by the Flux-Gate Magnetometer (FGM)<sup>43</sup> and particle data measured by Fast Plasma Investigation (FPI)<sup>41</sup> are used. The fluid bulk velocity is assumed to be equivalent to ion bulk velocity. The fluid density is calculated from ion number density  $\rho = N_i(m_i + m_e)$ , where  $m_i$  and  $m_e$  are mass of proton and electron, respectively. All data are in burst mode, and the sampling frequency of magnetic field and ions are 128 and 6.6 Hz, respectively, which has high time resolution to show details of turbulence. For constructing the gradient of magnetic field, the quantity measured by MMS 1–4 are interpolated onto the time grid of the magnetic field of MMS1.

Figures 2(a)–2(e) show the time signals of measurements belong to interval February 25, 2016 00:48 to 00:55. The number density of ions at mesocenter is shown in Fig. 2(a) with small fluctuations

TABLE I. The basic information of the data used in this study.

No.	Time interval	Location (GSE, Re)	$\langle N_i \rangle$ (cm <sup>-3</sup> )	$\langle V \rangle$ (km/s)	$ \langle \mathbf{B} \rangle $ (nT)	$B_{rms}/ \langle \mathbf{B} \rangle $	$\beta$
1	18-Oct-2015 14:57–15:10	(7.4, 8.6, -0.8)	9	232	38.8	0.34	1.26
2	21-Oct-2015 14:48–15:04	(7.7, 8.3, -0.8)	17	178	31.7	0.91	1.92
3	21-Oct-2015 15:33–15:56	(7.1, 8.3, -0.8)	13	139	31.9	0.84	2.24
4	04-Dec-2016 10:28–10:42	(11.0, 1.6, -1.0)	6	96	40.0	0.34	0.52
5	25-Feb-2016 00:48–00:55	(4.0, -10.3, -1.0)	30	151	52.6	0.18	0.68

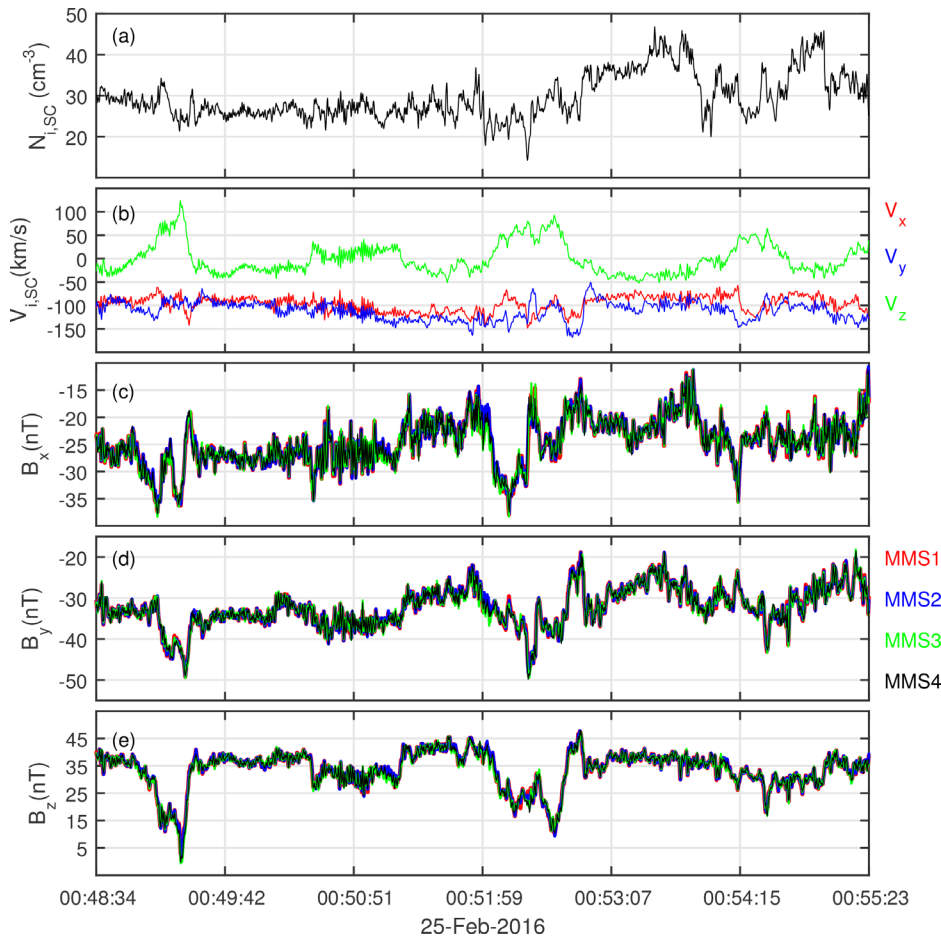


FIG. 2. Signals of data measured by MMS: (a) number density of ions, (b) bulk velocity of ions, and (c–e) components of magnetic field.

( $\Delta N_i \sim 5$ ) overlaid on a large scale variation from 20 to 50  $\text{cm}^{-3}$ . There also are abrupt declines and increments, implying a breaking up of incompressible assumption. Figure 2(b) shows the bulk velocity components of ions, showing that turbulent fluctuations have small magnitude. Large scale behavior of  $V_x$  and  $V_y$  are relatively stable, but there is about 100 km/s variation for  $V_z$  at 00:48:45 and 00:52:30, which may be due to magnetic reconnection process. The magnetic field components measured by FGM are shown in Figs. 2(c)–2(e). We can see that the fluctuation in magnetic field is weak, and the background field is dominant. The magnitudes of magnetic field components are close to each other. Large variations of  $B_z$  coincide with the variations of  $V_z$  in panel (b). Basic descriptions of data are shown in Table I. The mean values of ion number density ( $\langle N_i \rangle$ ), plasma bulk velocity, magnetic field intensity ( $\langle B \rangle$ ), and plasma beta  $\beta_{\perp}$  are different for five sets of data. Here,  $\beta$  is calculated based on normal pressure. The magnitudes of bulk velocity span from about 100–230 km/s, 100 times larger than spacecraft velocity, so that the motion of spacecraft can be ignored during observation.

Figures 3(a)–3(e) show the spectra of the ion bulk velocity magnitude and magnetic field of data table 1–5 used in this study. Here, x-axis represents the frequency that can be translated to wavenumber based on mean convective velocity, provided that Taylor hypothesis is valid.<sup>7,44</sup> In Figs. 3(a)–3(e), spanning from  $10^{-2}$  Hz to ion cyclotron

frequency ( $\Omega_i$ ), the scaling of both velocity and magnetic field exhibit a  $f^{-5/3}$  behavior, which proves that the data we have selected are in a strong turbulent state.<sup>45</sup> The scaling  $-5/3$  of the energy spectrum in the initial range of hydrodynamic case was first derived by Obukhov based on the isotropic, universal, and self-similar assumption of small scale turbulence; the core idea was established by Kolmogorov (K41).<sup>46</sup> For plasma turbulence, the condition is more complex. Because of the existence of large scale magnetic field, the interaction between small and large scale motion is not only through the eddies cascade but also through Alfvén waves, which results in a non-local interaction. Based on this picture and dimensional analysis, Iroshnikov and Kraichnan derived a  $k^{-3/2}$  spectrum.<sup>47</sup> When the frequency is larger than  $\Omega_i$ , the  $B$  spectrum becomes steeper and the spectrum of  $V$  becomes a plateau. The flatten of the  $V$  spectral power at higher frequencies indicates that the signal to noise ratio becomes too large and the measurements at these frequencies should not be trusted. More studies about spectral indices can be found in Ref. 7.

#### IV. RESULTS

Relying on the Lorentz force, the turbulent energy not only cascades in scale space but also transforms between fluid flow and magnetic field associated with the structure evolving. There is a particular current carrying structure, called force-free magnetic field configurations

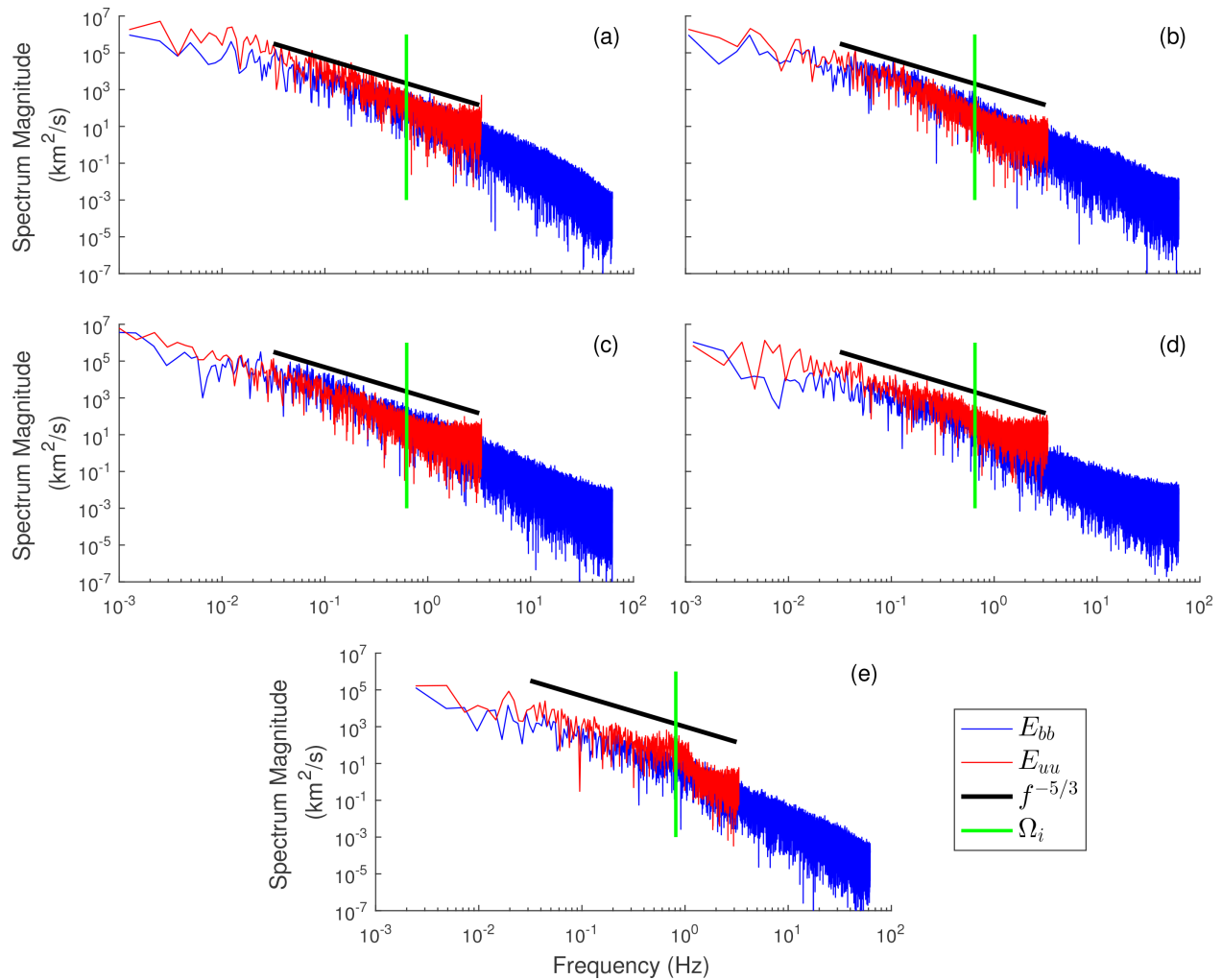


**FIG. 3.** Spectrums of the magnitude of ion bulk velocity (red line) and magnetic field (blue line). (a–e) correspond to data no. 1–5. The black line indicates scaling law  $\sim f^{-5/3}$ , and the green line is the ion cyclotron frequency calculated by  $\langle B \rangle$ , shown in Table I. The magnetic field signals are normalized by  $\sqrt{\rho\mu}$ , where  $\rho$  is density determined from  $\langle N_i \rangle$ , and  $\mu$  is permeability.

(FFMFC), that the direction of current density flux aligns with the direction of magnetic field resulting in zero Lorentz force. The FFMFC are also energy minimizing states under the condition of conservation of magnetic field helicity. Therefore, the FFMFC are stable and mainly advected by flow.<sup>48</sup> Here, we first focus on the distribution of the FFMFC in magnetosheath turbulence.

One simple criterion for diagnosing FFMFC is examining the angle between current density and magnetic field. Because current density equates to curl  $\mathbf{B}$  dividing permeability, the cosine of angle is as follows:

$$\zeta = \cos \alpha = \nabla \times \mathbf{B}_{SC} \cdot \mathbf{B}_{SC} / (|\nabla \times \mathbf{B}_{SC}| |\mathbf{B}_{SC}|), \quad (5)$$

where subscript SC means the mesocenter of MMS.

Figures 4(a) and 4(b) show the probability density of counts  $P(\zeta)$  involving all samples from data 1 to 5 in  $\zeta$  and  $\alpha$  space, respectively. The samples with  $|\zeta|$  larger than 0.94 are identified as FFMFC, which

are the same as Hnat *et al.*<sup>26</sup> We find about 23% of the samples is FFMFC being passively advecting, smaller than the proportion in solar wind, which is about 25%.<sup>26</sup> If the direction of current density is random and not affected by the direction of magnetic field, the PDF characterizing angle between the current density and the magnetic field should be constant in  $\alpha$  space, indicated by the red line in Figs. 4(a) and 4(b). Actually, the PDF computed from MMS data deviate from the ideal line, shown as the black line. The PDF is minimal at  $\zeta = 0$  ( $\alpha = \pi/2$ ) and increases with  $|\zeta|$ , reaching a maximum and decreases again at both ends. Figure 4(b) shows that the PDF loses symmetry when  $|\zeta|$  is larger than critical value (0.94), near  $\zeta = -1.0$  and less than  $\zeta = 1$ . This asymmetry cannot be explained by MHD theory, because MHD equations are invariant when  $\mathbf{B}$  turns to  $-\mathbf{B}$ . Therefore, the probability with the same  $|\zeta|$  should be the same. However, the parallel and anti-parallel current densities would generate different spiral magnetic field line, which may interact with

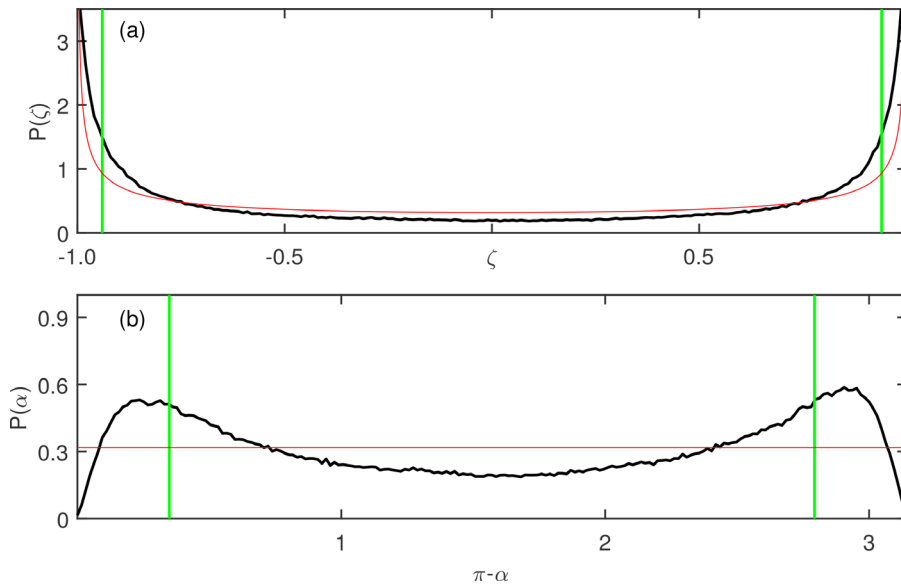


**FIG. 4.** (a) Probability density of counts  $P(\zeta)$  deduced from data 1–5. Green lines indicate  $|\zeta| = 0.94$ , the critical value to distinguish passive and active magnetic field configurations.<sup>26</sup>

electrons and protons differently, because electrons and protons move in magnetic field with different chirality. The lower probability at  $\zeta = -1$  may be related to the different interactions that the energy dissipation is easier through wave particle interaction near  $\zeta = -1$  than near  $\zeta = 1$ .

The distributions of sample number of FFMFC and non-FFMFC in  $(nR, nQ)$  plane are shown in Figs. 5(a) and 5(b), respectively. We separate the plane into grids with size  $0.1 \times 0.1$ , and the counts of samples in each grid is computed. The color of each grid is rendered according to its count, large count corresponding to red and small count corresponding to blue. Note that, every grid contains at least ten samples. The solid black line is the solution of  $D = 0$  in  $(nR, nQ)$  plane. Above the solid line,  $D$  is larger than zero, and below the solid line, the value of  $D$  is negative. For FFMFC, the total numbers of samples are about  $1.68 \times 10^5$ , of which more than 90% are distributed near  $nR = 0$  and  $nQ = 0$ . The samples of FFMFC have an inverted

calabash-shaped distribution with a statistical preference at  $nQ > 0$ . The proportion of  $D > 0$  is about 79.5%, and  $D < 0$  is about 20.5%. For non-FFMFC, the total numbers of samples are about  $3.89 \times 10^5$  and the distribution has a bell shape with a statistical preference at  $nQ < 0$ . Compared to FFMFC, non-FFMFC have a smaller proportion of  $D > 0$  about 70%, and  $D < 0$  about 30%. The different patterns of FFMFC and non-FFMFC shows that Lorentz force plays an important role in the dynamical evolution of magnetic field gradient.

According to the location in the  $(nR, nQ)$  plane, we can identify the topology of magnetic field structure of each sample.<sup>26</sup> For MHD flow, magnetic field intensity is also a factor that determines the topology in addition to the values of  $nR$  and  $nQ$ . The data used in this study are mainly located at the region of magnetosheath near the magnetopause where the magnetic field is strong. In the case of this situation, the dominant structures are flux ropes and recessive structures are flux tubes. For FFMFC, the percentage of flux ropes is 79.5% and flux tubes

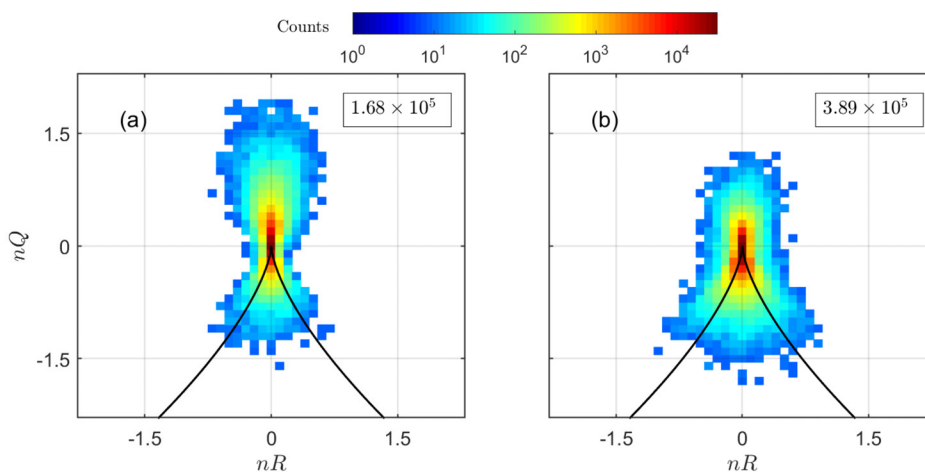


**FIG. 5.** Count distribution of samples in  $(nR, nQ)$  plane computed by data 1–5: (a) is for  $|\zeta| > 0.94$  corresponding to FFMFC and (b) is for  $|\zeta| \leq 0.94$ . Color bar denotes the counts, ranging from  $10^0$  to  $> 10^4$ .

is 20.5%. For non-FFMFC, the percentage of flux ropes is 70% and flux tubes is 30%. Note that both Figs. 5(a) and 5(b) are symmetric with respect to  $nR = 0$ , implying that there is no preference for right-hand or left-hand flux ropes and expanding or narrowing flux tubes. These patterns are different from the joint PDF of geometrical invariants of velocity field gradient that shows a tear drop region at  $R > 0, Q < 0$ , and  $R < 0, Q > 0$  quadrants, which is also the location where the most extreme events are found.<sup>24,30,49,50</sup>

It should be noted that the pattern of distribution of  $(nR, nQ)$  is similar to the results shown by Hnat *et al.*,<sup>26</sup> supporting that the turbulence in the magnetosheath is partly consistent with the solar wind. Hnat *et al.* use the following criterion for classification of topology,  $(D > 0, |nR| > 0.05)$  for plasmoids,  $(D > 0, |nR| < 0.05)$  for quasi-2D flux ropes, and  $(D < 0)$  for structures consistent with 3D neutral X-points. However, Hnat's classification cannot be applied to this study where data have strong guide field. We will try to determine the percentages of magnetosheath data satisfying the Hnat's criterion without considering specific structures. For FFMFC, samples for  $(D > 0, |nR| > 0.05)$ ,  $(D > 0, |nR| < 0.05)$ , and  $(D < 0)$  are in ratios 0.16:0.64:0.2, and for non-FFMFC, corresponding ratios are 0.10:0.60:0.30. The counterpart ratios in the solar wind are 0.19:0.54:0.27 for FFMFC and 0.09:0.52:0.39 for non-FFMFC.<sup>26</sup> The proportion of samples with  $|nR| < 0.05$  in the magnetosheath is obviously larger than that in the solar wind, which may be related to the strong magnetic field.

The Ohmic heating related to the current sheet is one channel for electron heating in collisionless space plasma turbulence.<sup>51</sup> In addition, both observation<sup>12</sup> and kinetic simulation<sup>52</sup> have shown that the term  $-(\mathbf{P} \cdot \nabla) \cdot \mathbf{V}$  is mostly responsible for converting a bulk flow into internal energy of the plasma. By investigating the distribution of mean current in  $(nR, nQ)$  plane, we can distinguish the role of different structures on electron heating. Figures 6(a) and 6(b) show the mean magnitude of the current density flux within different  $(nR, nQ)$  grid for FFMFC and non-FFMFC, respectively. The colors from blue to red denote the normalized intensity  $\langle j \rangle_{R,Q} / \sigma_j$ , where  $\sigma_j$  is the standard deviation of  $|j|$ ,  $\langle \cdot \rangle_{R,Q}$  denotes conditional average of samples located in  $(nR, nQ)$  grid. The maximum of  $\langle j \rangle_{R,Q} / \sigma_j$  is about five and minimum is about zero. It is obvious that intense currents mostly

occur at the edge of the pattern where  $nQ > 0$  in Figs. 6(a) and 6(b). The weak current mostly occurs at the neighborhood of  $(0, 0)$  where the field gradient is small. For non-FFMFC, the current density at  $D < 0$  region is evidently smaller than the current density at  $D > 0$ . We can conclude that the flux rope topologies are responsible for the dissipation of plasma turbulence since they carry large current, whereas the flux tube topologies carry little current. The patterns of current density distribution are similar with the results shown by Hnat *et al.*<sup>26</sup> Moreover, Fig. 6 provides more information on the intensity of current density. This shows that the intensity of current carried by FFMFC is larger than that carried by non-FFMFC, and non-FFMFC current density shows a stronger asymmetry with respect to  $D$  than FFMFC.

In MHD turbulence, the Lorentz force yielded by the action between large scale magnetic field and current plays a significant role in the non-local interaction. When the background field is strong, the small scale turbulence structures can be swept by the magnetic field, and cross-scale interaction occurs by counterpropagating waves.<sup>53</sup> Here, we investigate the distribution of decomposition of Lorentz force in  $nR - nQ$  plane. We decompose the Lorentz force into two terms as follows:

$$\mathbf{j} \times \mathbf{B} = \mathbf{B} \cdot \nabla \mathbf{B} - \nabla(\mathbf{B}^2/2), \tag{6}$$

where the first term can be regarded as surface stress, and the second term is magnetic pressure force. In addition,  $\mathbf{B} \cdot \nabla \mathbf{B}$  also characterizes how curved is the magnetic field line, that is why it is called tensile stress. Figures 7(a) and 7(b) show the conditional average  $\langle |\mathbf{B} \cdot \nabla \mathbf{B}| \rangle_{R,Q} / \sigma_f$  and  $\langle |\nabla(\mathbf{B}^2/2)| \rangle_{R,Q} / \sigma_f$  in each  $(nR, nQ)$  grid, respectively. Here, only non-FFMFC samples are considered,  $|\mathbf{x}| = \sqrt{x_1^2 + x_2^2 + x_3^2}$ , and  $\langle \cdot \rangle_{R,Q}$  denotes conditional average of samples in  $(nR, nQ)$  grid and  $\sigma_f$  is the standard deviation of Lorentz force intensity calculated by all non-FFMFC samples. Figure 7(a) shows that the tensile stresses tend to be strong at both sides and bottom of the pattern and decrease with  $nQ$  as  $nQ > 0$ . The intensity of the tensile stress near the right side of  $D = 0$  line seems larger than the left side of  $D = 0$  line. The reason resulting in this asymmetry is unknown. Figure 7(b) shows that the magnetic pressure forces tend to be strong

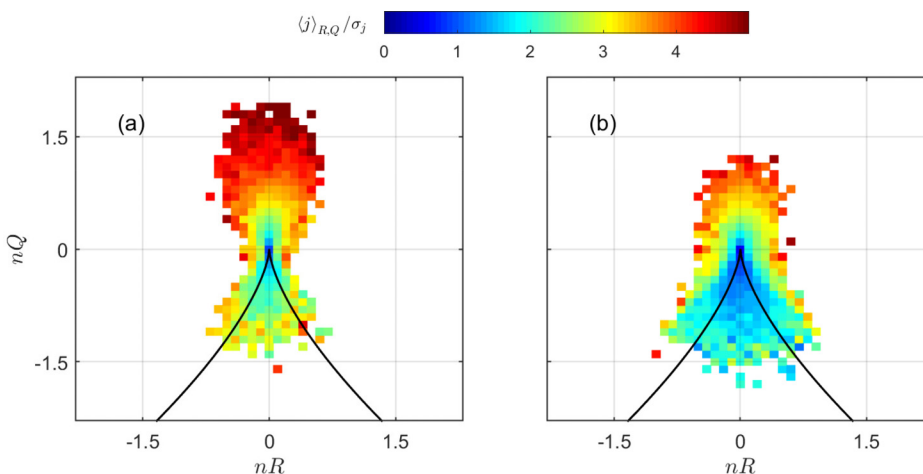


FIG. 6. Conditional average current density intensity in each  $(nR, nQ)$  grid for (a) FFMFC and (b) non-FFMFC.

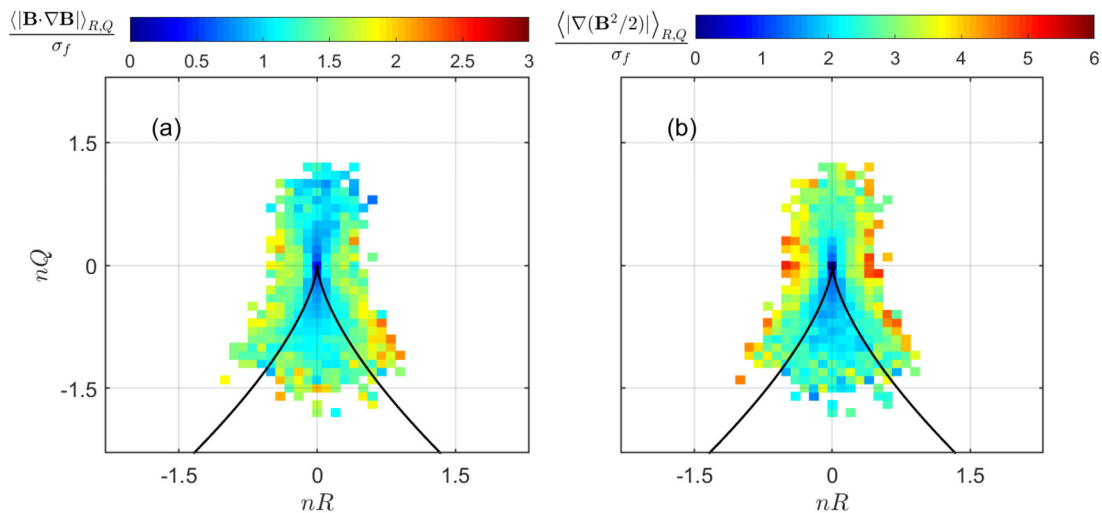


FIG. 7. Conditional average decomposition of Lorentz force in each  $(nR, nQ)$  grid for (a)  $\mathbf{B} \cdot \nabla \mathbf{B}$  and (b)  $\nabla(\mathbf{B}^2/2)$ .

at both sides and at the top of the pattern and increases with  $nQ$  as  $nQ > 0$ . Note that the color bar for magnetic pressure force ranges from 0 to 6, whereas the color bar for the tensile stress ranges from 0 to 3. The region where the current density is intensive, shown in Fig. 6(b), does not coincide with the strong force decomposition region shown in Figs. 7(a) and 7(b), implying that the angle between the current and the magnetic field is small for  $D > 0$  and  $nR \sim 0$  region.

## V. CONCLUSIONS

In summary, we analyzed the geometrical invariants of magnetic field gradient tensors and the distribution of current density and Lorentz decomposition in the  $(nR, nQ)$  plane using high-quality measurements from MMS in turbulent magnetosheath. In particular, we pointed out that the method for classification of velocity field topologies cannot be applied to the magnetic field directly because the large scale component of magnetic field cannot be removed by Galilean transformation, but the bulk velocity can be removed by Galilean transformation. In order to guarantee the analysis are reliable, we selected five sets of data in which MMS configuration meets nearly regular tetrahedron such that the ratios between minimum and maximum of the eigenvalues of the volume tensor are at least larger than 0.7. The typical  $-5/3$  spectrum associated with the turbulence cascade are validated by Fourier transform of the signal of the magnetic field and the ions' bulk velocity. By using the multiple point method, the full gradient tensor of  $\mathbf{B}$  is determined, and the corresponding invariant  $Q$  and  $R$  are calculated. The magnetic field structures are classified into FFMFC and non-FFMFC according to the angle between  $\mathbf{j}$  and  $\mathbf{B}$ . The percentage of FFMFC is about 23% and non-FFMFC is about 77%. Furthermore, relying on the distribution of samples in  $(nR, nQ)$  plane, the ratio of different magnetic field topologies is identified. For passive FFMFC structures, the flux ropes make up about 79.5%, which are dominated compared to the flux tubes (20.5%). For actively evolving structures, the proportion of flux tubes increases up to 30% of total samples, whereas the flux ropes cover up to 70%.

Furthermore, the distribution of current density and Lorentz force decomposition in  $(nR, nQ)$  are also investigated. It is evident that the flux ropes are dominant current carrying structures as compared to flux tubes. For the same  $(nR, nQ)$ , FFMFC structures carry more current density than non-FFMFC structures. The Lorentz force is decomposed into the tensile stress and the magnetic pressure force. The conditional average in  $(nR, nQ)$  plane shows that the flux ropes tend to associate with the magnetic pressure force; on the contrary, flux tubes tend to associate with the tensile stress of magnetic field lines. This result is helpful to identify the structures that are responsible for transporting energy directly from magnetosheath into the inner magnetosphere and ionosphere.

## ACKNOWLEDGMENTS

This work was supported by the National Natural Science Foundation (NSFC) of China (Grant Nos. 42130202 and 41874190), the Shenzhen Technology Project (JCYJ20190806144013077), and the National Key Research and Development Program of China (Grant No. 2022YFA1604600). We thank the MMS team for providing high-quality data on plasmas and field terms.

## AUTHOR DECLARATIONS

### Conflict of Interest

The authors have no conflicts to disclose.

### Author Contributions

**Yong Ji:** Conceptualization (equal); Data curation (equal); Investigation (equal); Methodology (equal); Writing – original draft (equal). **Chao Shen:** Funding acquisition (equal); Supervision (equal). **Lan Ma:** Data curation (equal); Writing – review & editing (equal). **Nian Ren:** Writing – review & editing (equal). **Nisar Ahmad:** Writing – review & editing (equal).

## DATA AVAILABILITY

The MMS data that support the findings of this study are openly available in MMS Science Data Center, <http://lasp.colorado.edu/mms/sdc/>.

## REFERENCES

- <sup>1</sup>Y. Zhou, "Turbulence theories and statistical closure approaches," *Phys. Rep.* **935**, 1–117 (2021).
- <sup>2</sup>W. H. Matthaeus, "Turbulence in space plasma: Who needs it?," *Phys. Plasmas* **28**, 032306 (2021).
- <sup>3</sup>C. Y. Tu and E. Marsch, "MHD structures, waves and turbulence in the solar wind: Observations and theories," *Space Sci. Rev.* **73**, 1–210 (1995).
- <sup>4</sup>S. Spangler, "Multi-scale plasma turbulence in the diffuse interstellar medium," *Space Sci. Rev.* **99**, 261–270 (2001).
- <sup>5</sup>H. Karimabadi, V. Roytershteyn, H. X. Vu, Y. A. Omelchenko, J. Scudder, W. Daughton, A. Dimmock, K. Nykyri, M. Wan, D. Sibeck, M. Tatineni, A. Majumdar, B. Loring, and B. Geveci, "The link between shocks, turbulence, and magnetic reconnection in collisionless plasmas," *Phys. Plasmas* **21**, 062308 (2014).
- <sup>6</sup>J. F. Drake, O. V. Agapitov, and F. S. Mozer, "The development of a bursty precipitation front with intense localized parallel electric fields driven by whistler waves," *Geophys. Res. Lett.* **42**, 2563–2570, <https://doi.org/10.1002/2015GL063528> (2015).
- <sup>7</sup>L. Rakhmanova, M. Riazantseva, and G. Zastenker, "Plasma and magnetic field turbulence in the Earth's magnetosheath at ion scales," *Front. Astron. Space Sci.* **7**, 115 (2021).
- <sup>8</sup>J. L. Burch, R. B. Torbert, T. D. Phan, L.-J. Chen, T. E. Moore, R. E. Ergun, J. P. Eastwood, D. J. Gershman, P. A. Cassak, M. R. Argall, S. Wang, M. Hesse, C. J. Pollock, B. L. Giles, R. Nakamura, B. H. Mauk, S. A. Fuselier, C. T. Russell, R. J. Strangeway, J. F. Drake, M. A. Shay, Y. V. Khotyaintsev, P.-A. Lindqvist, G. Marklund, F. D. Wilder, D. T. Young, K. Torkar, J. Goldstein, J. C. Dorelli, L. A. Avanov, M. Oka, D. N. Baker, A. N. Jaynes, K. A. Goodrich, I. J. Cohen, D. L. Turner, J. F. Fennell, J. B. Blake, J. Clemmons, M. Goldman, D. Newman, S. M. Petrinc, K. J. Trattner, B. Lavraud, P. H. Reiff, W. Baumjohann, W. Magnes, M. Steller, W. Lewis, Y. Saito, V. Coffey, and M. Chandler, "Electron-scale measurements of magnetic reconnection in space," *Science* **352**, aaf2939 (2016).
- <sup>9</sup>T. D. Phan, J. Eastwood, M. Shay, J. Drake, B. Sonnerup, M. Fujimoto, P. Cassak, M. Oieroset, J. Burch, R. Torbert, A. Rager, J. Dorelli, D. Gershman, C. Pollock, P. Sharma Pyakurel, C. Haggerty, Y. Khotyaintsev, B. Lavraud, Y. Saito, and W. Magnes, "Electron magnetic reconnection without ion coupling in Earth's turbulent magnetosheath," *Nature* **557**, 202 (2018).
- <sup>10</sup>J. Shuster, D. Gershman, J. Dorelli, B. Giles, S. Wang, N. Bessho, L.-J. Chen, P. Cassak, S. Schwartz, R. Denton, W. Uritsky, W. Paterson, C. Schiff, A. Viñas, J. Ng, L. Avanov, D. Silva, and R. Torbert, "Structures in the terms of the Vlasov equation observed at Earth's magnetopause," *Nat. Phys.* **17**, 1056–1065 (2021).
- <sup>11</sup>Y. Wang, R. Bandyopadhyay, R. Chhiber, W. Matthaeus, A. Chasapis, Y. Yang, R. Wilder, D. Gershman, B. Giles, C. Pollock, J. Dorelli, C. Russell, R. Strangeway, R. Torbert, T. Moore, and J. Burch, "Statistical survey of collisionless dissipation in the terrestrial magnetosheath," *J. Geophys. Res.* **126**, e2020JA029000, <https://doi.org/10.1029/2020JA029000> (2021).
- <sup>12</sup>R. Bandyopadhyay, W. H. Matthaeus, T. N. Parashar, Y. Yang, A. Chasapis, B. L. Giles, D. J. Gershman, C. J. Pollock, C. T. Russell, R. J. Strangeway, R. B. Torbert, T. E. Moore, and J. L. Burch, "Statistics of kinetic dissipation in the Earth's magnetosheath: MMS observations," *Phys. Rev. Lett.* **124**, 255101 (2020).
- <sup>13</sup>R. Bandyopadhyay, L. Sorriso-Valvo, A. Chasapis, P. Hellinger, W. H. Matthaeus, A. Verdini, S. Landi, L. Franci, L. Matteini, B. L. Giles, D. J. Gershman, T. E. Moore, C. J. Pollock, C. T. Russell, R. J. Strangeway, R. B. Torbert, and J. L. Burch, "In situ observation of Hall magnetohydrodynamic cascade in space plasma," *Phys. Rev. Lett.* **124**, 225101 (2020).
- <sup>14</sup>Z. S. She, E. Jackson, and S. Orszag, "Intermittent vortex structures in homogeneous isotropic turbulence," *Nature* **344**, 226–228 (1990).
- <sup>15</sup>B. Miao, B. Peng, and G. Li, "Current sheets from Ulysses observation," *Ann. Geophys.* **29**, 237–249 (2011).
- <sup>16</sup>L. Webster, D. Vainchtein, and A. Artemyev, "Solar wind discontinuity interaction with the bow shock: Current density growth and dawn-dusk asymmetry," *Sol. Phys.* **296**, 87 (2021).
- <sup>17</sup>M. Wan, W. H. Matthaeus, H. Karimabadi, V. Roytershteyn, M. Shay, P. Wu, W. Daughton, B. Loring, and S. C. Chapman, "Intermittent dissipation at kinetic scales in collisionless plasma turbulence," *Phys. Rev. Lett.* **109**, 195001 (2012).
- <sup>18</sup>L. Burlaga, R. Fitzenreiter, R. Lepping, K. Ogilvie, A. Szabo, A. Lazarus, J. Steinberg, G. Gloeckler, R. Howard, D. Michels, C. Farrugia, R. P. Lin, and D. E. Larson, "A magnetic cloud containing prominence material: January 1997," *J. Geophys. Res.* **103**, 277–285, <https://doi.org/10.1029/97JA02768> (1998).
- <sup>19</sup>J. Liu, Y. Gao, and C. Liu, "An objective version of the Rortex vector for vortex identification," *Phys. Fluids* **31**, 065112 (2019).
- <sup>20</sup>Y. Gao and C. Liu, "Rortex based velocity gradient tensor decomposition," *Phys. Fluids* **31**, 081704 (2019).
- <sup>21</sup>B. Sun, "A new additive decomposition of velocity gradient," *Phys. Fluids* **31**, 061702 (2019).
- <sup>22</sup>Y. Wu, W. Zhang, Y. Wang, Z. Zou, and J. Chen, "Energy dissipation analysis based on velocity gradient tensor decomposition," *Phys. Fluids* **32**, 035114 (2020).
- <sup>23</sup>M. S. Chong, A. E. Perry, and B. J. Cantwell, "A general classification of three-dimensional flow fields," *Phys. Fluids A* **2**, 765–777 (1990).
- <sup>24</sup>G. Consolini, M. Materassi, M. F. Marcucci, and G. Palocchia, "Statistics of the velocity gradient tensor in space plasma turbulent flows," *Astrophys. J.* **812**, 84 (2015).
- <sup>25</sup>V. Quattrocioni, G. Consolini, M. F. Marcucci, and M. Materassi, "On geometrical invariants of the magnetic field gradient tensor in turbulent space plasmas: Scale variability in the inertial range," *Astrophys. J.* **878**, 124 (2019).
- <sup>26</sup>B. Hnat, S. C. Chapman, and N. W. Watkins, "Magnetic topology of actively evolving and passively convecting structures in the turbulent solar wind," *Phys. Rev. Lett.* **126**, 125101 (2021).
- <sup>27</sup>J. Zhang, S. Huang, F. Sahraoui, N. Andrés, Z. Yuan, K. Jiang, S. Xu, Y. Wei, Q. Xiong, Z. Wang, R. Lin, and L. Yu, "Topology of magnetic and velocity fields at kinetic scales in incompressible plasma turbulence," *J. Geophys. Res.* **128**, e2022JA031064, <https://doi.org/10.1029/2022JA031064> (2022).
- <sup>28</sup>W. Matthaeus and M. Velli, "Who needs turbulence?," *Space Sci. Rev.* **160**, 145–168 (2011).
- <sup>29</sup>C. Shen, Z. J. Rong, M. W. Dunlop, Y. H. Ma, X. Li, G. Zeng, G. Q. Yan, W. X. Wan, Z. X. Liu, and C. M. Carr, "Spatial gradients from irregular, multiple-point spacecraft configurations," *J. Geophys. Res. Space Phys.* **117**, A11207, <https://doi.org/10.1029/2012JA018075> (2012).
- <sup>30</sup>H. M. Blackburn, N. N. Mansour, and B. J. Cantwell, "Topology of fine-scale motions in turbulent channel flow," *J. Fluid Mech.* **310**, 269–292 (1996).
- <sup>31</sup>V. Quattrocioni, G. Consolini, M. Materassi, T. Alberti, and E. Pietropaolo, "Lagrangian evolution of field gradient tensor invariants in magneto-hydrodynamic theory," *Chaos, Solitons Fractals* **9**, 100080 (2022).
- <sup>32</sup>M. Acuña, K. Ogilvie, D. Baker *et al.*, "The global geospace science program and its investigations," *Space Sci. Rev.* **71**, 5–21 (1995).
- <sup>33</sup>N. Olsen, G. Hulot, and T. Sabaka, "Measuring the Earth's magnetic field from space: Concepts of past, present and future missions," *Space Sci. Rev.* **155**, 65–93 (2010).
- <sup>34</sup>C. Shen, X. Li, M. Dunlop, Z. X. Liu, A. Balogh, D. N. Baker, M. Hapgood, and X. Wang, "Analyses on the geometrical structure of magnetic field in the current sheet based on cluster measurements," *J. Geophys. Res.* **108**, 1168, <https://doi.org/10.1029/2002JA009612> (2003).
- <sup>35</sup>C. Shen, X. Li, M. Dunlop, Q. Q. Shi, Z. X. Liu, E. Lucek, and Z. Q. Chen, "Magnetic field rotation analysis and the applications," *J. Geophys. Res.* **112**, A06211, <https://doi.org/10.1029/2005JA011584> (2007).
- <sup>36</sup>C. Shen, Z. J. Rong, and M. Dunlop, "Determining the full magnetic field gradient from two spacecraft measurements under special constraints," *J. Geophys. Res.* **117**, 018063, <https://doi.org/10.1029/2012JA018063> (2012).
- <sup>37</sup>C. Shen, C. Zhang, Z. Rong, Z. Pu, M. W. Dunlop, C. P. Escoubert, C. T. Russell, G. Zeng, N. Ren, J. L. Burch, and Y. Zhou, "Nonlinear magnetic gradients and complete magnetic geometry from multispacecraft measurements," *J. Geophys. Res.* **126**, e2020JA028846, <http://dx.doi.org/10.1029/2020JA028846> (2021).
- <sup>38</sup>C. Shen, Y. Zhou, Y. Ma, X. Wang, Z. Pu, and M. Dunlop, "A general algorithm for the linear and quadratic gradients of physical quantities based on 10 or more point measurements," *J. Geophys. Res.* **126**, e2021JA029121, <http://dx.doi.org/10.1029/2021JA029121> (2021).
- <sup>39</sup>Y. Y. Yang, C. Shen, Y. C. Zhang, Z. J. Rong, X. Li, M. Dunlop, Y. H. Ma, Z. X. Liu, C. M. Carr, and H. Rème, "The force-free configuration of flux ropes in geomagnetotail: Cluster observations," *J. Geophys. Res.* **119**, 6327–6341, <https://doi.org/10.1002/2013JA019642> (2014).

- <sup>40</sup>Y. Ji, C. Shen, N. Ren, L. Ma, Y. H. Ma, and X. Chen, "Curvature of magnetic field and its role on plasma in turbulent magnetosheath," *Astrophys. J.* **941**, 67 (2022).
- <sup>41</sup>C. Pollock, T. Moore, A. Jacques, J. Burch, U. Gliese, Y. Saito, T. Omoto, L. Avanov, A. Barrie, V. Coffey, J. Dorelli, D. Gershman, B. Giles, T. Rosnack, C. Salo, S. Yokota, M. Adrian, C. Aoustin, C. Auletta, S. Aung, V. Bigio, N. Cao, M. Chandler, D. Chornay, K. Christian, G. Clark, G. Collinson, T. Corris, A. De Los Santos, R. Devlin, T. Diaz, T. Dickerson, C. Dickson, A. Diekmann, F. Diggs, C. Duncan, A. Figueroa-Vinas, C. Firman, M. Freeman, N. Galassi, K. Garcia, G. Goodhart, D. Guererro, J. Hageman, J. Hanley, E. Hemminger, M. Holland, M. Hutchins, T. James, W. Jones, S. Kreisler, J. Kujawski, V. Lavu, J. Lobell, E. LeCompte, A. Lukemire, E. MacDonald, A. Mariano, T. Mukai, K. Narayanan, Q. Nguyen, M. Onizuka, W. Paterson, S. Persyn, B. Piepgrass, F. Cheney, A. Rager, T. Raghuram, A. Ramil, L. Reichenthal, H. Rodriguez, J. Rouzaud, A. Rucker, Y. Saito, M. Samara, J. A. Sauvaud, D. Schuster, M. Shappirio, K. Shelton, D. Sher, D. Smith, K. Smith, S. Smith, D. Steinfeld, R. Szymkiewicz, K. Tanimoto, J. Taylor, C. Tucker, K. Tull, A. Uhl, J. Vloet, P. Walpole, S. Weidner, D. White, G. Winkert, P. S. Yeh, and M. Zeuch, "Fast plasma investigation magnetospheric multiscale," *Space Sci. Rev.* **199**, 331–406 (2016).
- <sup>42</sup>C. Meneveau, "Lagrangian dynamics and models of the velocity gradient tensor in turbulent flows," *Annu. Rev. Fluid Mech.* **43**, 219 (2011).
- <sup>43</sup>C. T. Russell, B. J. Anderson, W. Baumjohann, K. R. Bromund, D. Dearborn, D. Fischer, G. Le, H. K. Leinweber, D. Leneman, W. Magnes, J. D. Means, M. B. Moldwin, R. Nakamura, D. Pierce, F. Plaschke, K. M. Rowe, J. A. Slavin, R. J. Strangeway, R. Torbert, C. Hagen, I. Jernej, A. Valavanoglou, and I. Richter, "The magnetospheric multiscale magnetometers," *Space Sci. Rev.* **199**, 189–256 (2016).
- <sup>44</sup>S. Y. Huang, L. Z. Hadid, F. Sahraoui, Z. G. Yuan, and X. H. Deng, "On the existence of the Kolmogorov inertial range in the terrestrial magnetosheath turbulence," *Astrophys. J. Lett.* **836**, L10 (2017).
- <sup>45</sup>A. Beresnyak, "MHD turbulence," *Living Rev. Comput. Astrophys.* **5**, 2 (2019).
- <sup>46</sup>A. Pouquet, U. Frisch, and J. Léorat, "Strong MHD helical turbulence and the nonlinear dynamo effect," *J. Fluid Mech.* **77**, 321–354 (1976).
- <sup>47</sup>P. D. Mininni, "Scale interactions in magnetohydrodynamic turbulence," *Annu. Rev. Fluid Mech.* **43**, 377–397 (2011).
- <sup>48</sup>P. A. Davidson, *An Introduction to Magnetohydrodynamics* (Cambridge University Press, 2001), pp. 95–96.
- <sup>49</sup>B. J. Cantwell, "Exact solution of a restricted Euler equation for the velocity gradient tensor," *Phys. Fluids A* **4**, 782 (1992).
- <sup>50</sup>J. Martín, A. Ooi, M. S. Chong, and J. Soria, "Dynamics of the velocity gradient tensor invariants in isotropic turbulence," *Phys. Fluids* **10**, 2336–2346 (1998).
- <sup>51</sup>H. Karimabadi, V. Roytershteyn, M. Wan, W. H. Matthaeus, W. Daughton, P. Wu, M. Shay, B. Loring, J. Borovsky, E. Leonardis, S. C. Chapman, and T. K. M. Nakamura, "Coherent structures, intermittent turbulence, and dissipation in high-temperature plasmas," *Phys. Plasmas* **20**, 012303 (2013).
- <sup>52</sup>Y. Yang, W. H. Matthaeus, S. Roy, V. Roytershteyn, T. N. Parashar, R. Bandyopadhyay, and M. Wan, "Pressure–strain interaction as the energy dissipation estimate in collisionless plasma," *Astrophys. J.* **929**, 142 (2022).
- <sup>53</sup>Y. Zhou, W. Matthaeus, and P. Dmitruk, "Colloquium: Magnetohydrodynamic turbulence and time scales in astrophysical and space plasmas," *Rev. Mod. Phys.* **76**, 1015–1035 (2004).